A coherent picture of the hydrogen oxidation and evolution reactions in aqueous solutions

Ershuai Liu[1], Li Jiao[2], Jingkun Li[1,3], Thomas Stracensky[1], Lynne Larochelle Richard[1], Qiang Sun[1], Sanjeev Mukerjee[1], and Qingying Jia*[,1]

[1]Department of Chemistry and Chemical Biology, Northeastern University, Boston, Massachusetts, 02115, United States

[2]Department of Chemical Engineering, Northeastern University, Boston, Massachusetts, 02115, United States

[3]Institut Charles Gerhardt Montpellier, UMR 5253, CNRS, Université Montpellier, ENSCM, Place Eugène Bataillon, 34095 Montpellier cedex 5, France

[1] is the previous address of J.L.; [3] is the present address.

*Correspondence authors. q.jia@northeastern.edu (Q. J.)

Abstract. Recent studies show the limitations of catalytic activity descriptor-based approaches to rationalize the kinetics of the hydrogen oxidation and evolution reactions (HOR/HER). Herein, we deposited several transition metals (TMs) onto Pt surfaces to disturb and probe the interface in alkaline solutions. The redox transition of these TMs in association with adsorption and desorption of reaction intermediates during the HOR/HER was monitored via *in situ* X-ray absorption spectroscopy. We propose that the TM facilitates the HOR by anchoring H_2O with the H-up configuration ($\uparrow H_2O_{ad}$) that removes H_{ad} on Pt via the bifunctional mechanism, based on the first in situ experimental evidence for the presence of $\uparrow H_2O_{ad}$ on surface Ru. Meanwhile, the TM promotes the HER of Pt by anchoring OH_{ad} to trigger the hard–soft acid–base (HSAB) mechanism for OH_{ad} removal. The revised 2B theory depicts a coherent picture of the HOR/HER kinetics in aqueous solutions.

Hydrogen oxidation and evolution reactions (HOR/HER) describe the electrochemical transformations between H_2 and water. They underlie the future hydrogen economy that relies on efficient consumption of H_2 such as in fuel cells and feasible production of H_2 from water such as in electrolyzers. In addition to their practical importance, the HOR/HER are the most fundamental electrochemical reactions. Studies of the HOR/HER kinetics in acidic solutions led to the establishment of underlying principles in electrochemistry such as the Butler-Volmer equation[1] and Sabatier's principle.[2] The HOR/HER activities of a broad range of elements in acidic solutions exhibit a volcano trend as a function of the metal-H binding energy (E_{M-H}), with Pt sitting near the top *as per* the Sabatier's principle.[3] However, this coherent picture of the HOR/HER kinetics in acidic solutions is not fully applicable when extending to alkaline solutions. The HOR/HER rates of several elements including Rh, Pd, Ir, Pt, and Au are all slower

in alkaline solution than in acid, no matter whether the E_{M-H} is too strong or weak, or nearly optimistic.[4] The breakdown of the Sabatier's principle in the HOR/HER kinetics across a wide pH range implicates that the volcano activity trend dictated by the E_{M-H} depicts only a limited scene of the HOR/HER, and a more general picture is to be discovered.

The HOR/HER rates of Pt not only slow down when switching from acidic to alkaline solutions, but also become sensitive to surface structures. For example, the alkaline HOR/HER kinetics of the Pt(110) facet is faster than that of Pt(111).[5] In addition, it was lately found that the HOR/HER rates of Pt surfaces other than Pt(111) (non-Pt(111)) are sensitive to alkali cations (AM^+) in alkaline solutions. The HOR/HER rates of non-Pt(111) surfaces decrease in the sequence of LiOH > NaOH > KOH.[6,7] Meanwhile, the HER improves whereas the HOR rate remains largely unchanged with increasing AM^+ concentration.[6,8-10] These AM^+-induced effects are, however, absent for the Pt(111) surface.[10,11] Moreover, the HOR/HER rates of Pt in alkaline solutions can be changed by decorating the Pt surface with a second transition metal (TM), and the change varies drastically depending on the identity of the TM. Surface Ru greatly improves the HOR/HER of Pt in alkaline solutions.[11-13] Surface Ni improves the HER markedly,[6,7,13,14] but HOR marginally,[6,7] whereas surface Co promotes the HER but lowers the HOR rate of Pt(111).[7] The high sensitivities of the HOR/HER rates of Pt in alkaline solutions to pH, surface structure, AM^+ identity and concentration, and TM identity have not been unified into a coherent picture by one theory.

Table 1 Summary of current theories for the HOR/HER.

	HER		HOR		
	Pt(111)	Non-Pt(111)	Pt(111)	Non-Pt(111)	Proposed theory
pH	√	√	√	√	pzfc[14], HBE[15]
AM^+ Identity	—	√	—	√	HBE[10], 2B[6]
AM^+ Conc.	—	√	—	—	Bifunctional[8], 2B[6]
TM	√	√	√	√	All[6,12-14,16]

— means ineffective, √ means effective.

Several theories have been proposed to account for these HOR/HER activity sensitivities (Table 1). Each of them works in some circumstances but fails in others. Koper *et al.*[14,17] proposed that the pH-dependent HOR/HER activity of Pt is caused by the pH-dependent potential of zero free charge (pzfc) that dictates the flexibility of water molecules in the inner-Helmholtz Plane (IHP) (pzfc theory). Whereas Yan *et al.*[15,18,19] ascribed it to the pH-dependent E_{Pt-H} (HBE theory). Markovic *et al.*[13,20,21] ascribed the slower HOR/HER kinetics of Pt in alkaline than in acidic solutions to the need to dissociate H_2O to provide H_{ad}. According to these arguments, the pH-induced change of the pzfc, HBE, or H_{ad} source affect both the HOR/HER as reversible reactions. These theories are thus theoretically plausible for the circumstances wherein the HOR/HER rates move together such as changing the surface structure, AM^+ identity, or adding surface Ru, but implausible for the cases that only the HER improves such as increasing AM^+ concentration[6] or inducing surface Co[7] (Table 1). We recently explained the AM^+-induced selective HER improvement as the hydrated AM^+ facilitate releasing the intermediate OH_{ad} into the bulk via the hard–soft acid–base (HSAB) theory: OH_{ad}-$[AM(H_2O)_x]^+$ + e^- → OH^--$[AM(H_2O)_x]^+$, and the surface Ni or Ru helps the HER in this regard by anchoring OH_{ad} to trigger the HSAB.[6] Accordingly, the surface Ni or Ru[12] induced-HOR improvement was ascribed to the bifunctional mechanism proposed by Markovic *et al.*[13] wherein the hosted OH_{ad} removes H_{ad}. This so-called 2B theory however fails to account for a recent finding by Tang's group[7] that the surface Co improves the HER but not the HOR of Pt in alkaline solutions, given that the Co can anchor OH_{ad} like Ni and thus shall improve the HOR. Moreover, the participation of OH_{ad} in the HOR/HER of Pt was ruled out by kinetics analysis.[22] Apparently, a universal theory that can account for all these circumstances is missing.

Herein, by depositing several TMs onto Pt surface to probe its HOR/HER interface in alkaline solutions with the help of X-ray absorption spectroscopy (XAS), we gave the first *in situ* experimental evidence for the specific adsorption of H_2O with the H-up configuration (denoted as $\uparrow H_2O_{ad}$) during the HOR. We accordingly propose that the HOR kinetics of non-Pt(111) surfaces in alkaline solutions is governed by the revised bifunctional mechanism wherein it is the $\uparrow H_2O_{ad}$ rather than OH_{ad} that oxidatively remove the H_{ad}. The revised 2B theory, which combines the revised bifunctional mechanism and the HSAB mechanism, appears to be compatible with all circumstances aforementioned, and gives a coherent picture of the HOR/HER kinetics in aqueous solutions.

The TM was electrochemically deposited onto a Pt polycrystalline electrode by immersing the electrode into the TM solution, following our previous protocol that allows for modulating the TM coverage on Pt surfaces by tuning the concentration of the solution.[6,12] The HOR/HER polarization curves of the bare and deposited electrode were obtained in a rotating disk electrode in a H_2-saturated 0.1 M KOH electrolyte. The TM-induced changes of the HOR/HER rates of Pt vary dramatically with the identity of TM, and accordingly are categorized into three quadrants in the Cartesian coordinate system, together with the representative polarization curves (Figure 1). Ru and Ni improve both the HOR/HER rates of Pt, in consistent with the literature.[11-14,20] Mn, Fe, and Co improve the HER but decrease the HOR rate of Pt, in agreement with Tang *et al*'s recent results.[7] In the case of 20 μM $Co(ClO_4)_2$ when the Co-induced blocking effect is insignificant as evidenced by the negligible change of the HOR limiting current density and the cyclic voltammetry (CV) (Figure S1), the significant HER rate improvement verifies that surface Co improves the HER kinetics of Pt, whereas the trivial decrease of the HOR rate suggests that Co has insignificant effects on the HOR kinetics other

than blocking the surface. Both the HOR/HER rates decrease for a higher Co coverage by increasing the concentration of $Co(ClO_4)_2$ to 100 µM because of the blocking effect (Figure 1, quadrant IV). Similarly, the HOR/HER rates of Pt slights decrease with 20 µM Cu^{2+}, and keep decreasing with increasing Cu^{2+} concentration (Figure 1, quadrant III), which indicates that surface Cu^{2+} also has negligible effects on the HOR/HER kinetics of Pt, and the decrease of the HOR/HER rates comes mainly from the blocking effect. Finally, selective improvement of the HOR without improving the HER is not seen here, or anywhere else.
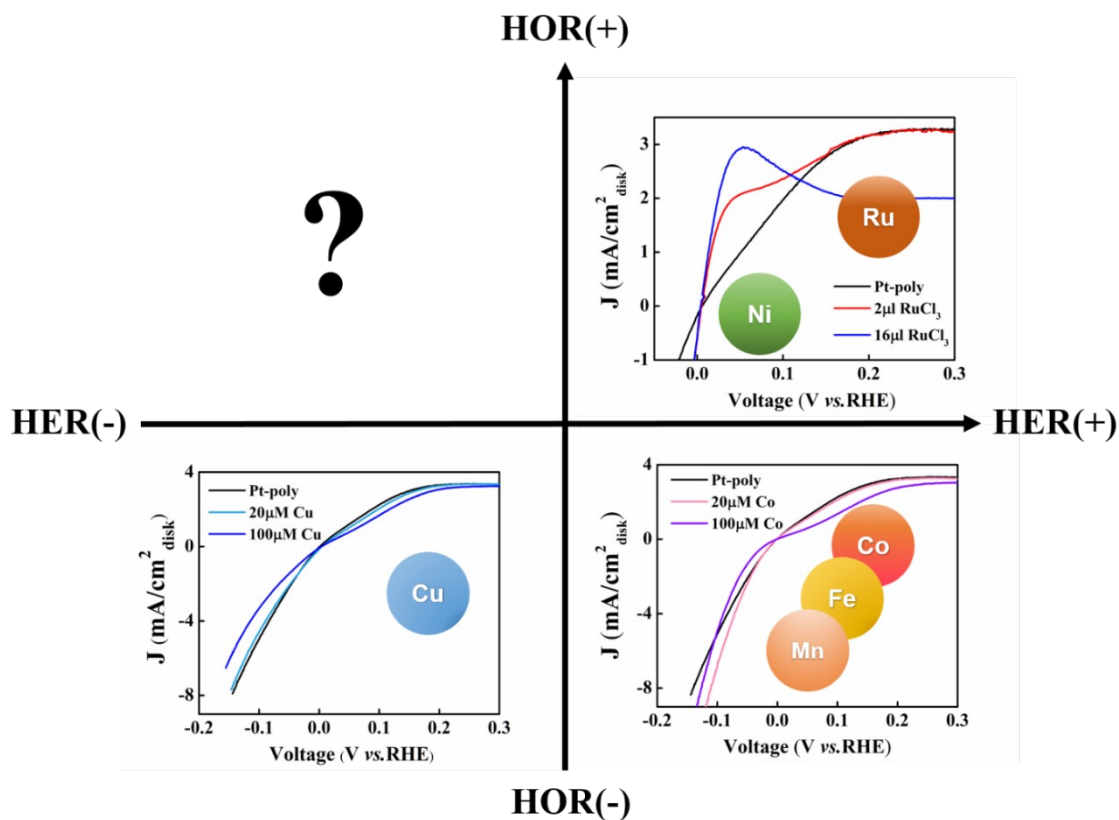

Figure 1. **TM-induced changes of the HOR/HER rates of Pt**. The HOR/HER polarization curves of the Pt polycrystalline electrode with/without surface deposition of Ru (quadrant I), Cu (quadrant III), and Co (quadrant IV) in an H_2-saturated 0.1 M KOH electrolyte at room temperature. Scan rate: 10 mV·s^{-1}. Rotation rate: 2,500 rpm.

The highly diversified TM-induced modifications of the HOR/HER rates of Pt in alkaline solutions indicate the different roles played by different TMs with different oxophicility in

affecting the HOR/HER kinetics of Pt. Accordingly, we conducted CO stripping experiments on the TM-deposited Pt electrode (except for Ru that is poisoned by CO[23]) since the TM oxophicility is known to play important roles in promoting the CO oxidation of Pt via the bifunctional mechanism.[20,24] The TM-induced improvement of the CO oxidation of Pt decreases in the order of Mn > Fe ~ Co > Ni > Cu (Figure 2a), in agreement with the trend previously acquired by depositing 3d metals onto Pt(111).[20] This trend consistently relates to the decreasing TMs' oxophicility in the same order, or equivalently the binding energy toward oxygen (E_{M-O}).[25] This trend is opposite to the HER trend of Mn < Fe ~ Co < Ni reported here (Figure 2b) and elsewhere,[7,20] except for Cu that has negligible effects on the HER kinetics of the Pt. These opposite trends can be rationalized by the reverse transport of hydroxyl throughout the IHP between the HER and CO oxidation (Figure 2). The HER involves releasing the TM-anchored OH_{ad} into the electrolyte forming OH^- *as per* the HSAB mechanism: OH_{ad}-$[AM(H_2O)_x]^+$+ e^- ↔ OH^--$[AM(H_2O)_x]^+$,[6] and is thus faster with weaker E_{M-O} until the E_{M-O} becomes too weak to effectively anchor OH_{ad} (like Cu) to trigger the HSAB. Reversely, the CO oxidation involves bringing OH^- from the electrolyte onto the surface TM forming OH_{ad}, and is faster with stronger E_{M-O}. This reasoning is further supported by the opposite trends of the HER and CO oxidation with AM^+ concentration and pH. We previously showed that the HER of Pt/C increases with increasing AM^+ concentration,[6] since the $[AM(H_2O)_x]^+$ facilitates the removal of OH_{ad}. This reasoning calls for the delay of the CO oxidation with increasing AM^+ concentration, which is indeed the case.[6] Furthermore, the slower HER kinetics of Pt in alkaline than in acid can be ascribed to the need to transport hydroxyl, accordingly the superior CO oxidation kinetics in alkaline than in acid[26] is attributable to the source of OH_{ad} directly from OH^- rather than water dissociation.
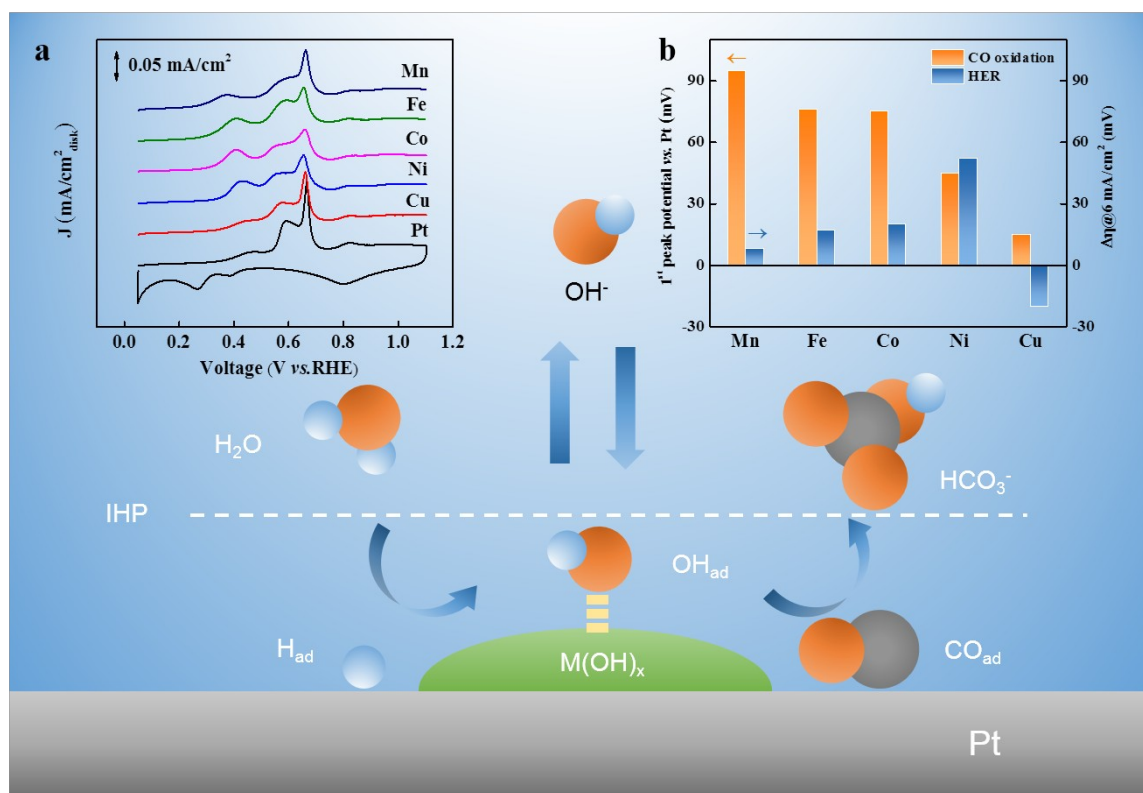
Figure 2. **The opposite transport of hydroxyl throughout the IHP between the HER and CO oxidation in alkaline solutions**. (**a**) Voltammetric profiles of CO stripping for Pt polycrystalline in an Ar-saturated 0.1 M KOH electrolyte with/without surface deposited TM (100 μM). Scan rate: 20 mV·s^{-1}. E_{ads} = 0.05 V (all potentials here are versus the reversible hydrogen electrode). (**b**) The TM-induced HER and CO oxidation improvement of Pt polycrystalline in a H$_2$- and Ar-saturated 0.1 M KOH electrolyte, respectively. Δη represents the improvement of HER overpotential when current density reaches 6 mA/cm^2. Original HER polarization curves were given in Figure S2.

While the CO stripping experiments support the presence of OH$_{ad}$ on the surface TMs, they defy the bifunctional mechanism wherein the TM-anchored OH$_{ad}$ removes the H$_{ad}$ on the Pt neighbors,[12,13] given that all the TMs improve the CO oxidation of Pt but only Ni improves the HOR. Even Ni facilitates both HOR and CO oxidation of Pt, the CO oxidation occurs above 0.3 V whereas the HOR improvement occurs below 0.1 V (Figure S3).[6] If the CO$_{ad}$ on Pt is removed by the OH$_{ad}$ on Ni, the H$_{ad}$ on Pt must not be removed by the same OH$_{ad}$. The potential dependent HOR improvement induced by Ni is also observed on Ru that improves the HOR of Pt below 0.15 V (Figure 1, quadrant I), which was previous observed by us,[12] and lately by Tang *et al*.[11] As

the Ru coverage increases, the HOR polarization curve reach the maximum around 0.05 V, and drops drastically with increasing potential (Figure 1, quadrant I). This curve closely resembles the HOR curve of Ru,[12,13] for which the drop is explained as the formation of hydr(oxy)oxides passivation layer. These results together suggest the Ni- or Ru-induced potential-dependent HOR improvement relates to its oxidation state that changes across the HOR/HER potential region.[6,12]

To monitor the dynamic oxidation states of the TMs deposited on Pt during the HOR/HER, *in situ* XAS was conducted at the K-edge of the TMs within the HOR/HER potential region in an H_2-saturated 0.1 M KOH electrolyte. As the potential increases, the X-ray absorption near edge structure (XANES) spectra of all the TMs shift to higher energy towards those of the corresponding (hydr)oxide standards, indicating the oxidation of TMs. The changes of the oxidation state of various TMs with increasing potentials were quantitatively compared (Figure 3d). This is enabled by choosing the energy at which the XANES spectrum is at 0.3 (E_{edge}) relative to those of the standards (STDs) to represent the oxidation state: $(n \times (E_{edge}(TM) - E_{edge}(STD^{0+}))/((E_{edge}(STD^{n+}) - E_{edge}(STD^{0+}))$ wherein n+ represents the valence of the STD (2+ for $Ni(OH)_2$), given that the oxidation state of TMs is nearly linearly related to the E_{edge}.[27] It is clearly seen that Co is dominated by $Co(OH)_2$ whereas Cu is dominated by metallic Cu^{0+} within the entire HER/HOR potential range. The increase of the oxidation state of Ni mainly occurs below 0 V, and $Ni(OH)_2$ dominates at positive potentials according to the XAS results we recently reported.[6] This redox transition agrees with the $Ni/Ni(OH)_2$ redox potential of 0.05 V in 0.1 M KOH.[28] Ru is dominated by metallic Ru^0 at negative potentials, and is progressively oxidized as the potential increases to 0.5 V (Figure 3c), which agrees well with the reversible $Ru/Ru(OH)_3$ transition between 0.2 – 0.8 V observed electrochemically.[29-31] Theses results show that the

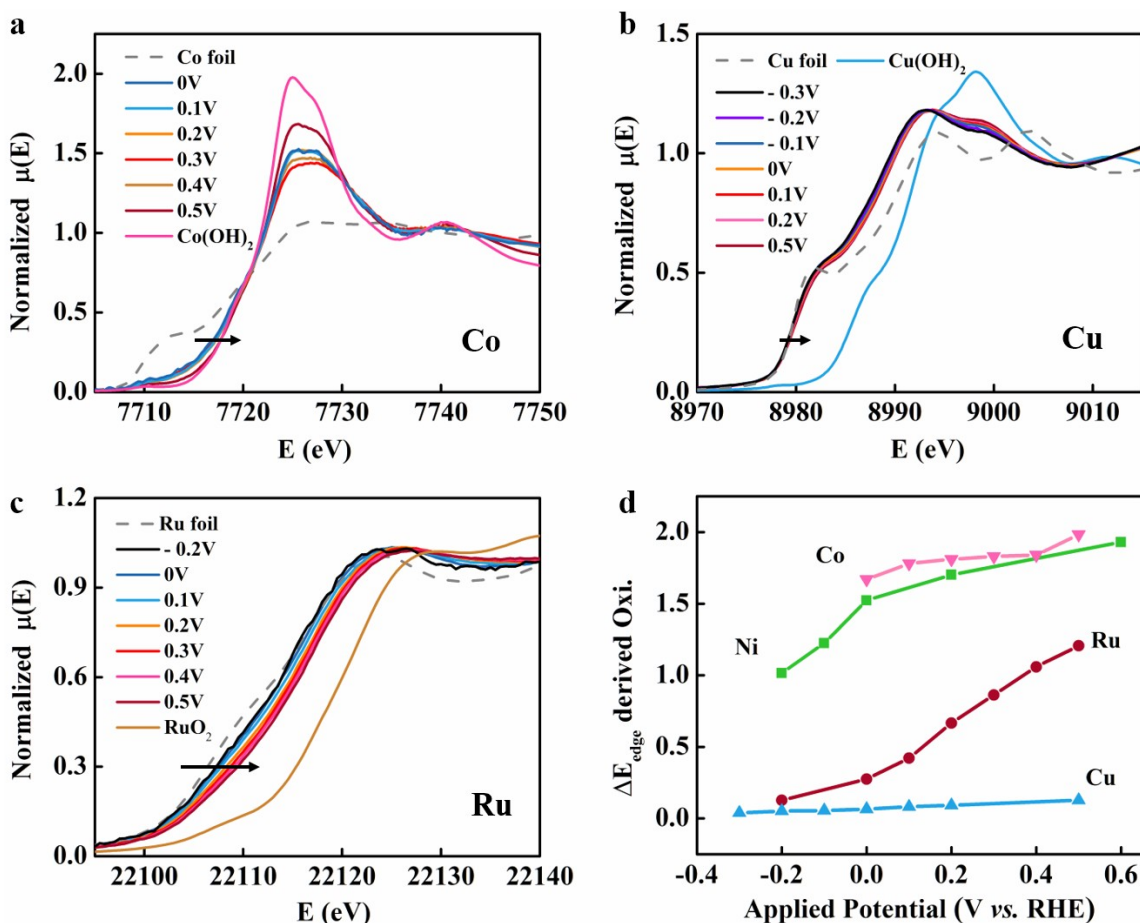phases and redox behaviors of these TMs are distinctly different within the HER/HOR potential

range.

Figure 3. **Redox transition of the TMs deposited on Pt/C reflected by XANES**. K-edge
XANES spectra of the (**a**) Co, (**b**) Cu, and (**c**) Ru deposited onto Pt/C as a function of applied
potentials collected in an H_2-purged 0.1 M KOH electrolyte. **(d)** The oxidation states of TMs
derived from the E_{edge} acquired from (a-c), and of Ni from our previous work.[6]

The Fourier Transform of the extended X-ray absorption fine structure (FT-EXAFS)

spectra of these TMs agree well with their corresponding XANES spectra. The deposited Co is

dominated by the Co-O (~1.5 Å) and Co-Co (~2.8 Å) peaks overlapping those of the Co(OH)$_2$

within the potential range of 0.1-0.5 V, and the Co-Co peak around 2.1 Å seen in the Co foil is

absent (Figure 4a). In contrast, a small Ni-Ni peak around 2.1 Å overlapping that of Ni foil is

clearly discernible at 0 V, and vanishes at positive potentials.[6] This reflects the presence of small

amounts of metallic Ni^0 phase at 0 V and its oxidation to $Ni(OH)_2$ at higher potentials. The FT-EXAFS spectra of Cu exhibit a prominent Cu-Cu peak around 2.1 Å overlapping that of the Cu foil (Figure 4b) between -0.3–0.5 V, which verifies the metallic Cu^0 as the dominate phase. A small Cu-O peak around 1.5 Å overlapping that of $Cu(OH)_2$ are discernible at positive potentials, indicating the mild oxidation of Cu^0 as also reflected by the minor XANES shift (Figure 3b).
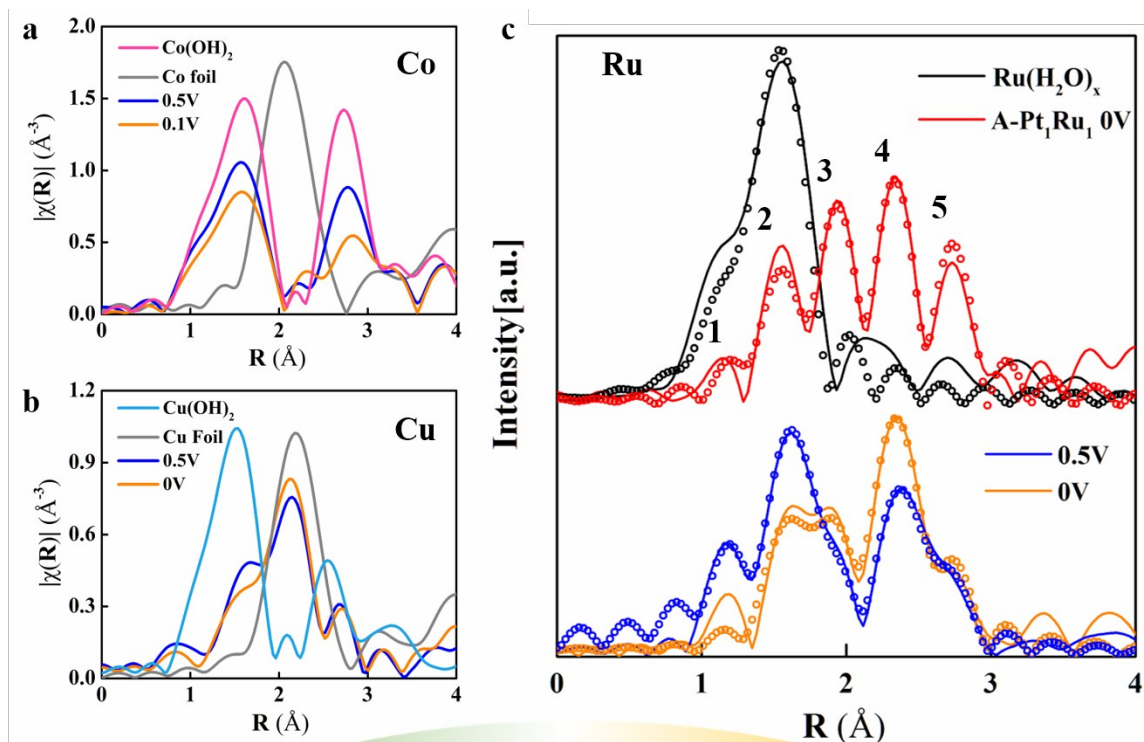
Figure 4. **Redox transition of TM^0/TM^{x+} during the HOR/HER**. K-edge FT-EXAFS spectra of the (**a**) Co, (**b**) Cu, and (**c**) Ru deposited onto Pt/C as a function of applied potentials collected in an H_2-purged 0.1 M KOH electrolyte. The scatter plots represent corresponding fittings of Ru. The fitting results were given in Table S1 and S2. The bottom scheme illustrates the two different bifunctional mechanism for the HER enabled by $\uparrow H_2O_{ad}$ and for the CO oxidation enabled by OH_{ad}.

Unlike Cu, the Ru FT-EXAFS spectrum at 0 V exhibits a prominent Ru-O peak around 1.5 Å, despite the predominate Ru^0 phase indicated by XANES. The five peaks, which are also observed in the Pt_1Ru_1 alloy (ETEK, 29.1 wt %) at 0 V, can be fitted with a Pt-Ru alloying model combined with a $Ru-O_x$ model (Figure 4c).[32] The fitting gives a coordination number of 3.1 ± 0.8 for the Ru-Pt bond, verifying the formation of the Pt-Ru alloying phase. A Ru-O bond with a coordination number of 0.9 ± 0.3 and bond length of 2.05 ± 0.02 Å is determined by fitting the scattering peak at 1.5 Å (Table S1). The assignment of this peak exclusively to the Ru-O bond in Ru hydr(oxy)oxides however conflicts with the XAENS spectrum that indicates the Ru^0 is the dominant phase. Furthermore, the Ru-O bond distance is longer than that of RuO_2 (1.97 ± 0.01 Å), but comparable to that of the $RuCl_3$ solution (2.04 ± 0.01 Å) wherein the Ru is coordinated by H_2O molecules (Table S3). We therefore assign this Ru-O peak at 0 V to the bonding between the metallic Ru^0 and the O from the specifically adsorbed $\uparrow H_2O$ molecules ($\uparrow H_2O_{ad}$-Ru). As the potential increases to 0.5 V, the intensities of the Ru-O peaks at 1.2 Å and 1.5 Å increase, whereas the intensities of the Ru-Ru/Pt peaks at 1.9 Å and 2.4 Å decrease. These results indicate the progressive adsorption of H_2O onto the surface Ru, followed by $\uparrow H_2O_{ad}$ dissociation leading to the formation of $Ru(OH)_3$ as the potential increases to 0.5 V.

The redox transition of Ru correlates well to the potential dependent Ru-induced improvement of the HOR of Pt (Figure 1). The HOR improvement is substantial at 0 V when the surface Ru is dominated by metallic Ru^0 that can anchor $\uparrow H_2O_{ad}$. The improvement gradually vanishes with the formation of $Ru(OH)_3$ as the potential increases. This correlation implicates

that it is the metallic Ru^0 rather than $Ru(OH)_3$ that improves the HOR of Pt. This implication is

applicable to other TMs. The marginal HOR improvement induced by the surface Ni below 0.1 V

is accompanied with the weak but discernible FT-EXAFS signals of Ni^0, and the $Ni/Ni(OH)_2$

redox potential of 0.05 V.[28] This redox-active behavior of Ni and Ru within the HOR kinetic

potential region of Pt clearly signifies their ability to attract the H_2O into the IHP forming

$\uparrow H_2O_{ad}$: $TM^0 + H_2O \leftrightarrow \uparrow H_2O_{ad}\text{-}TM^0 \leftrightarrow TM(OH)_x$. No HOR improvement was observed on Co

that is dominated by $Co(OH)_2$ with indiscernible Co^0 FT-EXAFS signals within the HOR

potential region, and Fe and Mn with even higher oxophicility. The Cu is dominated by Cu^0 that

is however incapable of anchor $\uparrow H_2O_{ad}$ before Pt reaches the HOR mass transport limit by 0.25

V,[33] as reflected by the indiscernible XAS signals of $\uparrow H_2O_{ad}\text{-}Cu$. Based on the foregoing

electrochemical and XAS results, we propose that it is the $\uparrow H_2O_{ad}$ anchored on metallic TM^0 that

removes the H_{ad} from the Pt for the HOR, whereas the OH_{ad} hosted on TM hydr(oxy)oxides

removes the CO_{ad} from the Pt for CO oxidation (Figure 4). As for the TM with a too low redox

potential of TM^0/TM^{x+} (denoted as V_{redox}) such as Mn, Fe, and Co, the metallic TM^0 phase is

absent at the HOR region and therefore it can't improve the HOR of Pt but improve the CO

oxidation. On the other hand, the TM with a too high V_{redox} such as Cu can't effectively anchor

$\uparrow H_2O_{ad}$ below 0.25 V and thus can't improve the HOR kinetics of Pt neither, but may improve the

CO oxidation at more positive potentials. Finally, the TM with a moderate V_{redox} such as Ni and

Ru improves the HOR kinetics of Pt within the potential region wherein it can anchor $\uparrow H_2O_{ad}$ but

without breaking it. The improvement vanishes with the dissociation of $\uparrow H_2O_{ad}$ leading to the

formation of hydr(oxy)oxides at more positive potentials.

      The revised bifunction mechanism describes that the surface TM facilitates the HOR of

Pt in alkaline solutions by anchoring $\uparrow H_2O_{ad}$ that releases the intermediate H_{ad}. Meanwhile, the

HSAB mechanism we proposed previously[6] describes that the surface TM improves the HER of Pt by anchoring the intermediate OH_{ad} that is later released by $[AM(H_2O)_x]^+$. The combined 2B theory implicates that the sluggish HOR/HER kinetics of Pt in alkaline solutions is limited by the transport of reaction intermediates, in line with the pzfc theory.[14] The pzfc theory fully accounts for the pH-dependence of the HOR/HER kinetics of Pt(111)[14] that cannot host $\uparrow H_2O_{ad}$ or OH_{ad} within the HOR/HER potential region[34] so the 2B theory is inapplicable, and the H_{ad} or OH^- is transported by $\uparrow H_2O$ with the orientation dictated solely by the pzfc. Resultantly, the HER/HOR kinetics of Pt(111) is unaffected by AM^+ identity and concentration.[10] The pzfc also accounts for the pH-dependent HOR/HER rates of non-Pt(111) surfaces such as Pt(110), but the 2B theory also applies since the Pt(110) can anchor $\uparrow H_2O_{ad}$ or OH_{ad} within the HOR/HER potential region,[34] due probably to the higher surface charge[35] and/or stronger E_{M-O}[36] with lower coordination numbers. This explains why the HOR/HER kinetics of Pt(110) is superior to that of Pt(111).[5] The sensitivity of the HER of non-Pt(111) to AM^+ identity and concentration in alkaline solutions is manifested by the HSAB mechanism.[6] The HOR is insensitive to AM^+ concentration since the HSAB mechanism is irrelevant. It is sensitive to AM^+ identity because the $\uparrow H_2O_{ad}$ competes with H_{ad} for Pt sites. As the $\uparrow H_2O_{ad}$-Pt binding energy in alkaline solutions decreases in the order of $Li^+ > Na^+ > K^+$,[34] the $\uparrow H_2O_{ad}$ replaces H_{ad} at more positive potentials, delaying the bifunctional HOR. In this regard, the 2B theory agrees with the refined HBE theory wherein the comparative binding energy between the Pt-H_{ad} and $\uparrow H_2O_{ad}$-Pt dictates the HOR activity of Pt.[19] An important implication derived from this argument is that the sharp underpotential-deposited hydrogen (H_{UPD}) desorption peak of stepped Pt surfaces or Ru is caused by the replacement of H_{ad} by $\uparrow H_2O_{ad}$, but rather than OH_{ad}.[34] Accordingly, the H_{UPD} peak of stepped Pt surfaces at lower potential in LiOH than in KOH signifies the early replacement of H_{ad} by $\uparrow H_2O_{ad}$ and thus better

HOR kinetics, whereas the absence of the H_{UPD} peak for Pt(111) signifies the absence of ↑H_2O_{ad} within the H_{UPD} region.

The coherent picture of the HOR/HER kinetics of Pt in aqueous solutions depicted by the combined 2B theory and pzfc theory underlines the importance of H_2O in transporting reaction intermediates. In principle, this study shows that the interface matters.

Methods

Chemicals. Carbon supported platinum nanoparticles (Pt/C, 47.2 wt.%) were purchased from Tanaka Kikinzoku Kogyo. Copper(II) perchlorate hexahydrate ($Cu(ClO_4)_2·6H_2O$, 98%), nickel(II) perchlorate hexahydrate ($Ni(ClO_4)_2·6H_2O$, 99.99%), cobalt(II) perchlorate hexahydrate ($Co(ClO_4)_2·6H_2O$, 99%), iron(III) perchlorate hydrate ($Fe(ClO_4)_3·H_2O$, crystalline, low chloride), manganese(II) perchlorate hydrate ($Mn(ClO_4)_2·xH_2O$, 99%), potassium hydroxide (KOH, 99.99%), perchloric acid ($HClO_4$, 70%, PPT Grade) were all purchased from Sigma-Aldrich. All aqueous solutions were prepared using deionized (DI) water (18.2 MΩ·cm) obtained from an ultra-pure purification system (Aqua Solutions).

Electrode preparation. Prior to the electrodeposition, the glass carbon electrode embedded in PTFE or the Pt polycrystalline electrode was polished mechanically by 0.5 µm, 0.3 µm, 0.05 µm alumina powder and then sonicated in sequence for 5 minutes in DI water and ethanol.

Electrochemical measurements. All the electrochemical experiments were conducted using a three-electrode cell system. Pt wire and Ag/AgCl (1 M Cl⁻) reference electrode were used as the counter and reference electrodes respectively. All potentials reported in this paper are referenced to the reversible hydrogen electrode (RHE), calibrated in the same electrolyte by measuring the potential of the HOR/HER currents at zero corresponding to 0 V versus RHE (V_{RHE}).

Prior to the RDE testing in alkaline, Pt polycrystalline electrode were cycled with a rotation rate of 1,600 rpm in an Ar-saturated 0.1 M $HClO_4$ electrolyte with a scan rate of 500 mVs^{-1} between the potential range of 0.05 - 1.2 V_{RHE} for 100 cycles following the Department of Energy (DOE) recommended protocol.[37] Typical experimental procedures for HER/HOR experiments can be referred to our previous work.[6]

Impedance measurements: the impedance spectra were measured with frequencies from 10^5 to 0.1 Hz with amplitude of 10 mV by Autolab. Equivalent circuits were fitted to the data with Zview software.

Electrochemical deposition of M(ClO$_4$)$_2$ （M=Mn, Co, Ni, Cu）, Fe(ClO$_4$)$_3$ and RuCl$_3$: after the CV and HER/HOR measurements of the Pt polycrystalline, the electrode was unmounted from the RDE and immersed in 20 µM $M(ClO_4)_2$ for 1 minute. Then the HER/HOR polarization curves and the CV were recorded in a H_2/Ar-saturated 0.1 M KOH electrolyte under identical conditions as those of Pt polycrystalline. This process was repeated with increasing concentration of $M(ClO_4)_2$ until 100 µM. Electrochemical deposition for $RuCl_3$ deposition followed our previous study.[12]

CO stripping. Before conducting the CO stripping experiments, two potential cycles between 0.05 and 1.1 V_{RHE} in 0.1 M KOH with scan rate of 20 mV·s^{-1} were applied to the electrode before the adsorption of carbon monoxide by dosing the gas at a constant potential of 0.05 V_{RHE} for 5 minutes into the solution, and then Ar was purged into the same electrolyte for 25 minutes at the same potential to remove the CO from the electrolyte.

In situ XAS data collection and analysis. The preparation method of the XAS electrodes can be referred to our previous work.[38,39] The final Pt geometric loadings were chosen to give 0.5 transmission spectra edge heights at the Pt L_3 edge. The XAS experiments were conducted at

room temperature in a previously described flow half-cell in which continuously H_2-purged 0.1 M KOH was circulated. The voltage cycling limits were -0.3 to 0.6 V_{RHE}. The data at the Cu and Co edges of the Pt/C immersed in $Cu(ClO_4)_2$, $Co(ClO_4)_2$ solutions were collected in the fluorescence mode at the beamline ISS 8-ID, the data at the Ru edge of Pt/C immersed in $RuCl_3$ were collected in 7-BM and the data of RuO_2 standard were collected in 6-BM of the National Synchrotron Light Source (NSLS) II, Brookhaven National Laboratory (BNL). Typical experimental procedures were utilized with details provided in our previous work.[38,39]

References

1. Erdey-Gruz, T. & Volmer, M. The theory of hydrogen overvoltage. *Z. Phys. Chem* **150**, 203 (1930).

2. Trasatti, S. Work function, electronegativity, and electrochemical behaviour of metals: III. Electrolytic hydrogen evolution in acid solutions. *J. electroanal. chem. interfacial electrochem.* **39**, 163-184 (1972).

3. Skúlason, E. *et al.* Modeling the electrochemical hydrogen oxidation and evolution reactions on the basis of density functional theory calculations. *J. Phys. Chem. C* **114**, 18182-18197 (2010).

4. Herranz, J. *et al.* Interfacial effects on the catalysis of the hydrogen evolution, oxygen evolution and CO_2-reduction reactions for (co-)electrolyzer development. *Nano Energy* **29**, 4-28 (2016).

5. Schmidt, T. J., Ross, P. N. & Markovic, N. M. Temperature dependent surface electrochemistry on Pt single crystals in alkaline electrolytes: Part 2. The hydrogen evolution/oxidation reaction. *J. Electroanal. Chem.* **524-525**, 252-260 (2002).

6. Liu, E. *et al.* Unifying the hydrogen evolution and oxidation reactions kinetics in base by identifying the catalytic roles of hydroxyl-water-cation adducts. *J. Am. Chem. Soc.* **141**, 3232-3239 (2019).

7. Rebollar, L., Intikhab, S., Snyder, J. D. & Tang, M. H. Determining the viability of hydroxide-mediated bifunctional HER/HOR mechanisms through single-crystal voltammetry and microkinetic modeling. *J. Electrochem. Soc.* **165**, J3209-J3221 (2018).

8. Danilovic, N. *et al.* The Effect of noncovalent interactions on the HOR, ORR, and HER on Ru, Ir, and $Ru_{0.50}Ir_{0.50}$ metal surfaces in alkaline environments. *Electrocatalysis* **3**, 221-229 (2012).

9. Subbaraman, R. *et al.* Enhancing hydrogen evolution activity in water splitting by tailoring Li+-Ni (OH) 2-Pt interfaces. *Science* **334**, 1256-1260 (2011).

10. Strmcnik, D. *et al.* The role of non-covalent interactions in electrocatalytic fuel-cell reactions on platinum. *Nat. Chem.* **1**, 466 (2009).

11. Intikhab, S. *et al.* Exploiting dynamic water structure and structural sensitivity for nanoscale electrocatalyst design. *Nano Energy* **64**, 103963 (2019).

12. Li, J. *et al.* Experimental proof of the bifunctional mechanism for the hydrogen oxidation in alkaline media. *Angew. Chem. Int. Ed.* **56**, 15594-15598 (2017).

13. Strmcnik, D. *et al.* Improving the hydrogen oxidation reaction rate by promotion of hydroxyl adsorption. *Nat. Chem.* **5**, 300-306 (2013).

14. Ledezma-Yanez, I. *et al.* Interfacial water reorganization as a pH-dependent descriptor of the hydrogen evolution rate on platinum electrodes. *Nat. Energy* **2**, 17031 (2017).

15. Sheng, W. *et al.* Correlating hydrogen oxidation and evolution activity on platinum at different pH with measured hydrogen binding energy. *Nat. Commun.* **6** (2015).

16. Lu, S. & Zhuang, Z. Investigating the influences of the adsorbed species on catalytic activity for hydrogen oxidation reaction in alkaline electrolyte. *J. Am. Chem. Soc.* **139**, 5156-5163 (2017).

17. Van der Niet, M. J., Garcia-Araez, N., Hernández, J., Feliu, J. M. & Koper, M. T. Water dissociation on well-defined platinum surfaces: The electrochemical perspective. *Catal. Today* **202**, 105-113 (2013).

18. Zheng, J., Sheng, W., Zhuang, Z., Xu, B. & Yan, Y. Universal dependence of hydrogen oxidation and evolution reaction activity of platinum-group metals on pH and hydrogen binding energy. *Sci. Adv.* **2** (2016).

19. Zheng, J., Nash, J., Xu, B. & Yan, Y. Perspective—towards establishing apparent hydrogen binding energy as the descriptor for hydrogen oxidation/evolution reactions. *J. Electrochem. Soc.* **165**, H27-H29 (2018).

20. Subbaraman, R. *et al.* Trends in activity for the water electrolyser reactions on 3d M (Ni, Co, Fe, Mn) hydr(oxy)oxide catalysts. *Nat. Mater.* **11**, 550-557 (2012).

21. Danilovic, N. *et al.* Enhancing the alkaline hydrogen evolution reaction activity through the bifunctionality of Ni(OH)$_2$/metal catalysts. *Angew. Chem. Int. Ed.* **51**, 12495-12498 (2012).

22. Intikhab, S., Snyder, J. D. & Tang, M. H. Adsorbed hydroxide does not participate in the volmer step of alkaline hydrogen electrocatalysis. *ACS Catal.* **7**, 8314-8319 (2017).

23. Marković, N. M. & Ross, P. N. Surface science studies of model fuel cell electrocatalysts. *Surf. Sci. Rep.* **45**, 117-229 (2002).

24. Watanabe, M. & Motoo, S. Electrocatalysis by ad-atoms: Part II. Enhancement of the oxidation of methanol on platinum by ruthenium ad-atoms. *J. electroanal. chem. interfacial electrochem.* **60**, 267-273 (1975).

25. Rankin, R. B. & Greeley, J. Trends in selective hydrogen peroxide production on transition metal surfaces from first principles. *ACS Catal.* **2**, 2664-2672 (2012).

26. García, G. Correlation between CO oxidation and H adsorption/desorption on Pt surfaces in a wide ph range: the role of alkali cations. *ChemElectroChem* **4**, 459-462 (2017).

27. Jia, Q. *et al.* Metal and metal oxide interactions and their catalytic consequences for oxygen reduction reaction. *J. Am. Chem. Soc.* **139**, 7893-7903 (2017).

28. Sheng, W., Myint, M., Chen, J. G. & Yan, Y. Correlating the hydrogen evolution reaction activity in alkaline electrolytes with the hydrogen binding energy on monometallic surfaces. *Energy Environ. Sci.* **6**, 1509-1512 (2013).

29. Juodkazytė, J., Vilkauskaitė, R., Stalnionis, G., Šebeka, B. & Juodkazis, K. EQCM study of Ru and RuO_2 surface electrochemistry. *Electroanalysis* **19**, 1093-1099 (2007).

30. Sugawara, Y., Yadav, A., Nishikata, A. & Tsuru, T. EQCM study on dissolution of ruthenium in sulfuric acid. *J. Electrochem. Soc.* **155**, B897-B902 (2008).

31. Povar, I. & Spinu, O. Ruthenium redox equilibria 3. Pourbaix diagrams for the systems Ru-H_2O and Ru-Cl-H_2O. *Journal of Electrochemical Science and Engineering* **6**, 145-153 (2016).

32. Alayoglu, S. *et al.* Structural and architectural evaluation of bimetallic nanoparticles: a case study of Pt−Ru core−shell and alloy nanoparticles. *ACS Nano* **3**, 3127-3137 (2009).

33. Sheng, W., Gasteiger, H. A. & Shao-Horn, Y. Hydrogen oxidation and evolution reaction kinetics on platinum: acid vs alkaline electrolytes. *J. Electrochem. Soc.* **157**, B1529-B1536 (2010).

34. McCrum, I. T. & Janik, M. J. pH and alkali cation effects on the pt cyclic voltammogram explained using density functional theory. *J. Phys. Chem. C* **120**, 457-471 (2016).

35. Abbas, Z., Labbez, C., Nordholm, S. & Ahlberg, E. Size-dependent surface charging of nanoparticles. *J. Phys. Chem. C* **112**, 5715-5723 (2008).

36. Calle-Vallejo, F. *et al.* Finding optimal surface sites on heterogeneous catalysts by counting nearest neighbors. *Science* **350**, 185-189 (2015).

37. Kocha, S. S. *et al.* Best practices and testing protocols for benchmarking orr activities of fuel cell electrocatalysts using rotating disk electrode. *Electrocatalysis* **8**, 366-374 (2017).

38. Jia, Q. *et al.* Activity descriptor identification for oxygen reduction on platinum-based bimetallic nanoparticles: in situ observation of the linear composition–strain–activity relationship. *Acs Nano* **9**, 387-400 (2015).

39. Jia, Q. *et al.* Circumventing metal dissolution induced degradation of Pt-alloy catalysts in proton exchange membrane fuel cells: revealing the asymmetric volcano nature of redox catalysis. *ACS Catal.* **6**, 928-938 (2016).